

High-efficiency catalyst for copper nanoparticles attached to porous nitrogen-doped carbon materials: Applied to the coupling reaction of alkyne groups under mild conditions

Lei Ma  | Pengbo Jiang  | Kaizhi Wang  | Xiaokang Huang  |
Ming Yang  | Li Gong  | Rong Li 

State Key Laboratory of Applied Organic Chemistry (SKLAOC), the Key Laboratory of Catalytic Engineering of Gansu Province, College of Chemistry and Chemical Engineering, Lanzhou University, Lanzhou, China

Correspondence

Rong Li, State Key Laboratory of Applied Organic Chemistry (SKLAOC), the Key Laboratory of Catalytic Engineering of Gansu Province, College of Chemistry and Chemical Engineering, Lanzhou University, Lanzhou, Gansu 730000, China.
Email: liyirong@lzu.edu.cn

Supported catalysts have attracted extensive attention due to their excellent catalytic performance and reliability in heterogeneous catalysis. In this work, we report a general synthesis strategy that achieves the self-coupling reaction of acetylene derivatives to 1,3-diyne efficiently under conditions of copper catalyst impregnated on the precursor formed by acetone and urea. The experiments were performed by screening the base, solvent, temperature, and so forth to determine the optimum reaction conditions and then characterization and analysis of the catalyst. The results demonstrate that the Cu/CuO@CN(8) exhibits extraordinary reactivity to the self-coupling reaction and achieves a high turnover frequency (TOF = 96.8). Typically, the conversion of phenylacetylene reaches 99.9% under the optimal reaction conditions of NaOH (2 mmol) and tert-butanol (2 ml) and O₂ (1 atm) at 60°C for 1 h. Nevertheless, it is worth noting that Cu/CuO@CN(8) has a large specific surface area (626.07 m² g⁻¹) and low metal loading (3.3%) measured by Brunauer Emmett-Teller (BET) and ICP-OES, respectively. Simultaneously, kinetics and mechanism are also discussed and analyzed, and the thermodynamic energy value is calculated as 22.74 kJ mol⁻¹. Besides, the optimum catalyst can be reused five times under optimal conditions without a significant decrease in reactivity.

KEYWORDS

1,3-dynes, coupling reaction, heterogeneous catalysis, kinetic study, phenylacetylene

1 | INTRODUCTION

Transforming aromatic alkyne into 1,3-diyne releases its enormous value as an organic monomer. 1,3-diyne is a kind of conjugated diyne compound with symmetric and asymmetric structure and unique properties, which are widely applied to material chemistry and synthetic chemistry because of its antibacterial, anti-inflammatory, and anticancer effects.^[1] At the same time, 1,3-diyne is also an important part of photovoltaic materials,

electromagnetic materials, and optical devices.^[2] Because the initial synthesis strategy has some shortcomings, such as low atom utilization, failure to achieve reuse, and complex reaction conditions.^[3] Therefore, the conversion from homogeneous catalysis to heterogeneous catalysis and performance improvement of heterogeneous catalysts are significant topics in the current research field (Table S1).^[4]

Due to the maturity of the reactions and complexity of the products, the Glaser-Hay coupling reaction

attracted the attention of many scientists in recent years and had become one of the vital strategies for organic synthesis.^[5] In the past few decades, terminal alkynyl groups showed outstanding talent in various fields.^[6] Palladium-, copper-catalytic systems have been successfully developed to achieve self-coupling of terminal alkynes.^[7] It is worth noting that copper is considered cheaper and easier to obtain than palladium at the same conversion rate.^[8] Besides, limited research was conducted on the recyclability and high efficiency of the catalysts used in this reaction, which remains a hot topic in current research.^[9] In addition, the copper (I) salt (e.g., CuI and CuCl) has been reported in a large number of previous catalytic systems, which is a challenge to overcome the shortcoming in the recycling of the catalyst.^[10] To address the above issues, various strategies have been dedicated to achieve load reduction based on reducing the band gap and accelerating the separation of electron-hole pairs and increasing their catalytic activity.^[2a,10b] With the development of a series of related researches, its synthetic process has become more and more simple and efficient. Nitrogen-doped carbon materials are considered as a well carrier with high surface area, better stability, and electrical conductivity.^[11] The lone pair of nitrogen can modify the copper nanoparticles on the surface of the support and fix the Cu nanoparticles, which increases the recyclability of the catalyst.^[12] In addition, Cu catalyst doped with N has been extensively studied in the coupling reaction. Therefore, research on supported metal catalysts has important significance. Indeed, this type of catalysts was reported by many researches because of its high efficiency, recyclability, and simplicity.^[10c,13]

Herein, this work focuses on Glaser-Hay reaction, and phenylacetylene is used as a starting material to construct 1,4-diphenylbutadiyne.^[14] A type of high-surface-area polyporous and coral-like carbon materials was synthesized from acetone^[15] and applied to synthetic 1,4-diphenylbutadiyne under mild reaction conditions.^[16] Optimal reaction conditions were obtained by analyzing the factors, such as alkali, solvent, reaction temperature, and reaction time. Experimental exploration shows the prepared catalyst has a high surface area ($656 \text{ m}^2 \text{ g}^{-1}$), and the Cu nanoparticles are uniformly dispersed on the surface of the carrier. Moreover, the catalyst produces high conversion (99.9%) under conditions of 60°C and O_2 (1 atm). Compared with the activities of the copper salt catalysts, the cycle performance can be maintained at least five times without significant reaction decay. Furthermore, the kinetics of the exploration also illustrates the rationality of the catalyst.

2 | EXPERIMENTAL SECTION

2.1 | Reagents and chemicals

All the reagents and chemicals used in the synthesis of catalyst were purchased from commercial sources and used without further purification, unless otherwise noted.

Detailed description of the reagents and chemicals will be displayed in the support information.

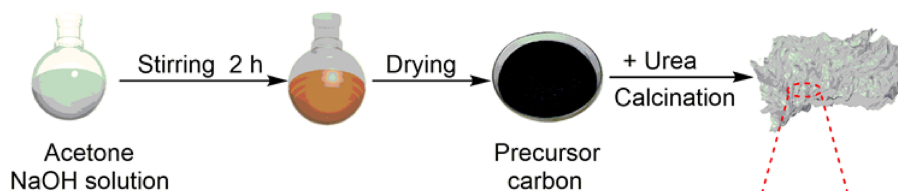
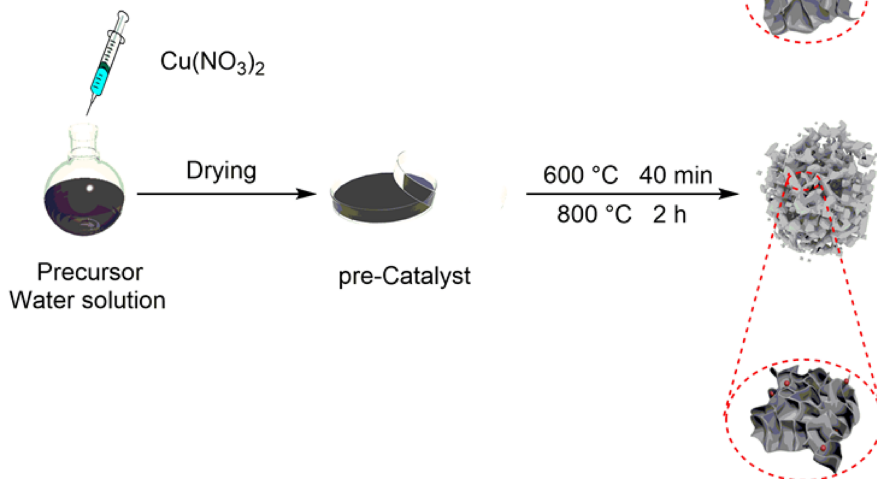
2.2 | Preparation of N-doped porous carbon precursor (CN)

For the synthesis of porous carbon-based materials (Scheme SCHEME 1), initially, acetone (40 ml) and sodium hydroxide (8 g) were added to a one-necked 100 ml round-bottomed flask equipped with a mechanical stirrer. Subsequently, the mixture will be sonicated for 30 min at room temperature. Since then, the reaction was carried out in a water bath at 40°C , which isolated the air and stirred vigorously for 2 h. After the reaction, it was gradually cooled to room temperature. The color of the mixture changes from colorless to orange during this reaction.

A mixture of urea (3 g) and carbon precursor (1 g) in agate mortar was completely ground for 10 min and followed transferred to a quartz boat. Later, the sample was calcined at 800°C for 2 h with a heating rate of 3°C min^{-1} in a tube furnace under N_2 flow. After the end of calcination, the system was cooled to room temperature naturally and the black powder was obtained. Furthermore, the sample was washed several times with deionized water and hydrochloric acid (1 M, 62 ml) until the solution become neutral. Subsequently, the mixture was separated by filtration. Finally, the precursor was obtained by drying at 60°C for 24 h and named by CN.

2.3 | Preparation of the Cu/CuO@CN catalyst

An interconnected solid matrix with polyporous was synthesized directly by immobilizing the Cu salts ($\text{Cu}(\text{NO}_3)_2 \cdot 3\text{H}_2\text{O}$, $\text{CuSO}_4 \cdot 5\text{H}_2\text{O}$, $\text{Cu}(\text{CH}_3\text{COO})_2 \cdot \text{H}_2\text{O}$, $\text{CuCl}_2 \cdot 2\text{H}_2\text{O}$) on the surface of CN (Scheme SCHEME 1). The preparatory work before the synthesis was as follows: Different copper salts (0.03 M) and deionized water (30 ml) were added to a 100-ml beaker, and the mixture was stirred continuously for 20 min to allow the solid precipitate to be dissolved thoroughly. Subsequently, the prepared solution (1 M) was transferred to a 100-ml conical flask.

SCHEME 1 Preparation of the carbon materials and catalysts**1. Synthesis of carbon precursor (CN)****2. Synthesis of catalysts**

Next, the CN (400 mg) was suspended in 35-ml deionized water. The copper nitrate solution (1.65 ml) was added gradually to the suspension and followed by slight stirring at 100°C for 3 h in an oil bath. The reaction was carried out until the deionized water was completely evaporated. After removing deionized water in air, the mixture was collected and dried at 60°C in a vacuum oven. Latterly, the catalyst was first calcined under a N₂ flow of 60 ml min⁻¹ at 600°C for 40 min in a tube furnace, followed by increasing the temperature to 800°C for 2 h with a heating rate of 3°C min⁻¹. After cooling to room temperature, the Cu/CuO@CN catalyst was obtained.

Preparation of Cu/CuO@C by the same synthesis method as Cu/CuO@CN without N, and samples with different Cu content were obtained with labeled as Cu/CuO@CN (*x*%), where *x* stands for the Cu/CN mass ratio in the composite. So the Cu/CuO@CN (6.5%), Cu/CuO@CN (12%), and Cu/CuO @ CN (20%) are synthesized in this experiment. In addition, Cu/CuO@CN (6), Cu/CuO@CN (7), and Cu/CuO@CN (9) were also prepared separately by converting the highest temperature of the second heating process to 600°C, 700°C, and 900°C. Moreover, other different types of copper salts were synthesized by the same method and named Cu/CuO@CN (S), Cu/CuO@CN (C), and Cu/CuO@CN (Cl), respectively.

2.4 | Catalytic evaluation

According to a typical process, the coupling reaction was carried out in a 10-ml grinding tube filled with oxygen (1 atm). To the mixture were added catalyst (20 mg), NaOH (80 mg, 2 mmol) and phenylacetylene (102 mg, 1 mmol) in tert-Butanol (2 ml) was heated at 60°C for 1 h with magnetic stirring. Subsequently, the sample was extracted with deionized water (2 × 3 ml) and ethyl acetate (1 × 1 ml). Later, the product was collected by centrifugation then analyzed and determined by gas chromatography–mass spectrometry (GC–MS) (Agilent 6890N/5937N). The activity of the catalyst was calculated as follows: conversion % = 100 × (([C₀] – [C₁])/[C₀]), yield % = 100 × (2 × [C₂]/[C₀]), and TOF = ([C₀] – [C₁]) × V / (M_{Cu}) / *t*. Based on the initial concentration [C₀] and the remaining concentration [C₁] of the reactant, as well as the concentration of the resulting product [C₂], *V* represents the volume of the solvent in the system, and the reaction time is represented by *t*. In addition, M_{Cu} is expressed as the molar amount of Cu in the catalyst.

2.5 | Characterizations

To understand the physical and chemical properties of the catalyst in more detail. Some measurement methods

would be applied as follows: X-ray diffraction (XRD), X-ray photoelectron spectroscopy (XPS), high-angle annular dark-field scanning transmission electron microscopy (HAADF-STEM), Brunauer Emmett-Teller (BET), elemental analysis (EA), Fourier-transform infrared spectroscopy (FT-IR), Raman spectra, and inductively coupled plasma optical emission spectrometer (ICP-OES). A detailed description of the catalyst characterization instrument would be provided in the supporting information.

3 | RESULTS AND DISCUSSION

3.1 | Characterization of catalysts

The crystal structure and phase composition of the catalysts were systematically investigated by using XRD patterns and Raman spectra. The XRD results of the precursor and the catalyst are shown in Figure 1. Notably, the two broad smooth peaks are shown in the nitrogen-doped precursor (CN). The two strong peaks are orthorhombic of the catalyst, and the positions of peaks at 36° and 43° correspond to the (111) and (111) planes, which shows a typical pattern of crystalline Cu particles (JCPDS no. 70-3038) and CuO particles (JCPDS no. 3-884). The patterns of other types of Cu-based catalysts by the same method show five peaks at 36° , 43° , 50° , 61° , and 74° , which correspond to the (111), (111), (200), (220), and (220) planes, respectively (Figure S1).

At the same time, because the catalyst is a carbon-based composite, the Raman scattering spectroscopy shows detailed defect information for the CN and catalyst (Figure 1b). The characteristic D-band and G-band of graphitized carbon correspond to two peaks at

approximately 1360 and 1590 cm^{-1} , respectively, illustrating the formation of structural defects in the graphitic plane and the E_{2g} vibrational mode of the sp^2 -bond graphitic carbons. The intensity of the D and G bands (I_D/I_G) indicates the degree of graphitization of the carbon material. Furthermore, the I_D/I_G value increased from 0.968 to 1.0243 with the temperature rising from 600°C to 800°C . However, when the temperature rose to 900°C , the value drops to 1.0076. Therefore, it can be concluded that the highest I_D/I_G value can be attributed to Cu/CuO@CN(8), and this indicates that its structure has a large defect concentration. In addition, Raman of CN and Cu/CuO@CN (8) are also shown in Figure S2, which indicates that the degree of graphitization of the carbon material is not significantly changed by the introduction of the metal.

In order to obtain further detailed information on the morphology and microstructures of the CN, as well as the dispersion of metal particles on the precursor, the scanning electron microscope (SEM) technique is employed. As shown in Figure 2a and 2b, the SEM images demonstrates that the CN is a petal-like structure. It can be confirmed that the precursor has a porous structure from Figure 2c. At the same time, the topography of Cu/CuO@CN(8) is also shown in Figure 2d, and it can be observed that the structure of the carbon material is slightly altered by doping the metal, but the porous, petal-like structure in the catalyst is still clearly visible. This may be attributed to the second calcination. Besides, it can be clearly seen that the metal particles are uniformly dispersed on the catalyst surface. In addition, the SEM is also used for the catalyst and support after the cycles (Figure S3). Figure S3a-S3c and Figure S3d-S3f reflect the changes in the morphology of the catalyst after two and five cycles, respectively. Through observation of

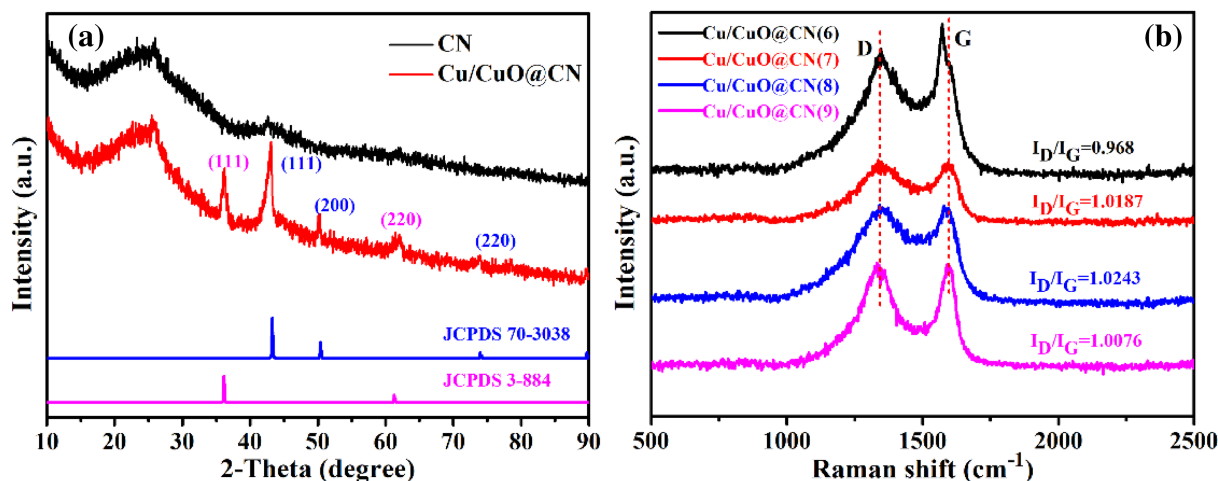


FIGURE 1 (a) X-ray diffraction (XRD) pattern of the CN and Cu/CuO@CN and (b) Raman spectra of different catalysts

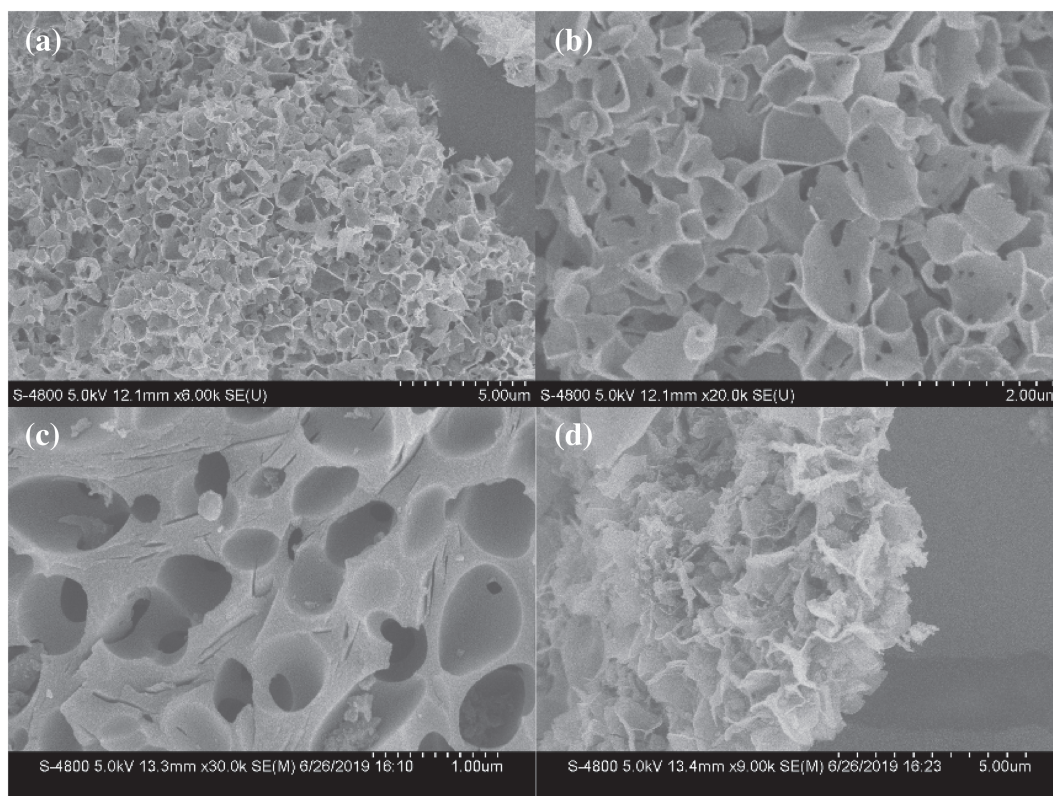


FIGURE 2 (a–c) Scanning electron microscope (SEM) image of the CN and (d) scanning electron microscope (SEM) image of the Cu/CuO@CN(8)

Figure S3a–S3c, which can be seen that the morphology of the catalyst did not change significantly after two cycles, it still appeared petal-like, with only a small amount of flake structure broken (Figure S3c). Although the petal-like structure gradually changed—a little collapse and the active components in the catalyst fell off a little, resulting in a decrease in the activation rate after five cycles, the overall catalytic activity remains well—the conversion rate is still above 90%.

Meanwhile, the transmission electron microscopy (TEM) images (Figure 3a and 3b) also demonstrate that the Cu/CuO@CN(8) catalyst is a kind of petal-like material with a unique porous structure and the wall of hole is composed of the nanosheets, which is consistent with the SEM image of Cu/CuO@CN(8) (Figure 2d). TEM image of the Cu/CuO@CN(8) is shown in Figure 3a and 3b. From Figure 3a, the topography of the carbon material is changed slightly when nitrogen is incorporated, which is more like a kind of three-dimensional nanorod structure. As shown in Figure 3b, the structure of the catalyst is converted from a petal shape to a sheet shape by calcination with supported metal. The particle size distribution image is shown in Figure S4, and it can be observed that the metal nanoparticles are uniformly distributed on the precursor. In addition, it can be

concluded that the particle size of the Cu nanoparticles is approximately 2–5 nm, and the size is 3–4 nm account for 40% of all the particles. At the same time, the average size of the nanoparticles is calculated to be approximately 3.8 nm (inset in Figure S4). The results of the high-resolution TEM (HR-TEM) image (magnified image of Figure S4) are Figure 3c, which further indicate that the lattice fringe spacing is d_1 (0.206 nm) and d_2 (0.245 nm) corresponds to the 111, 111 crystal planes of Cu, CuO in the target catalyst, respectively. Furthermore, they are matched to diffraction peaks at 36° and 43° for XRD results, respectively. HAADF-STEM acts as a specific area of the element mapping shown in Figure 3g. Besides, the elemental mapping of the catalyst indicates that C, N, and Cu are uniformly distributed over a particular region, thereby inferring that the Cu nanoparticles are homogeneously dispersed on the N-doped carbon material (Figure 3d–3f). However, the content of Cu (Figure 3f) is less than of C and N, which is attributed to the lesser amount introduced in the process of synthesizing the catalyst. In addition, the optimal catalyst is also characterized after the cycles (Figure S5). It can be observed that the general morphology of the petals remains unchanged after several cycles—the morphology of the petals remains obvious. Figure S5b still shows that copper

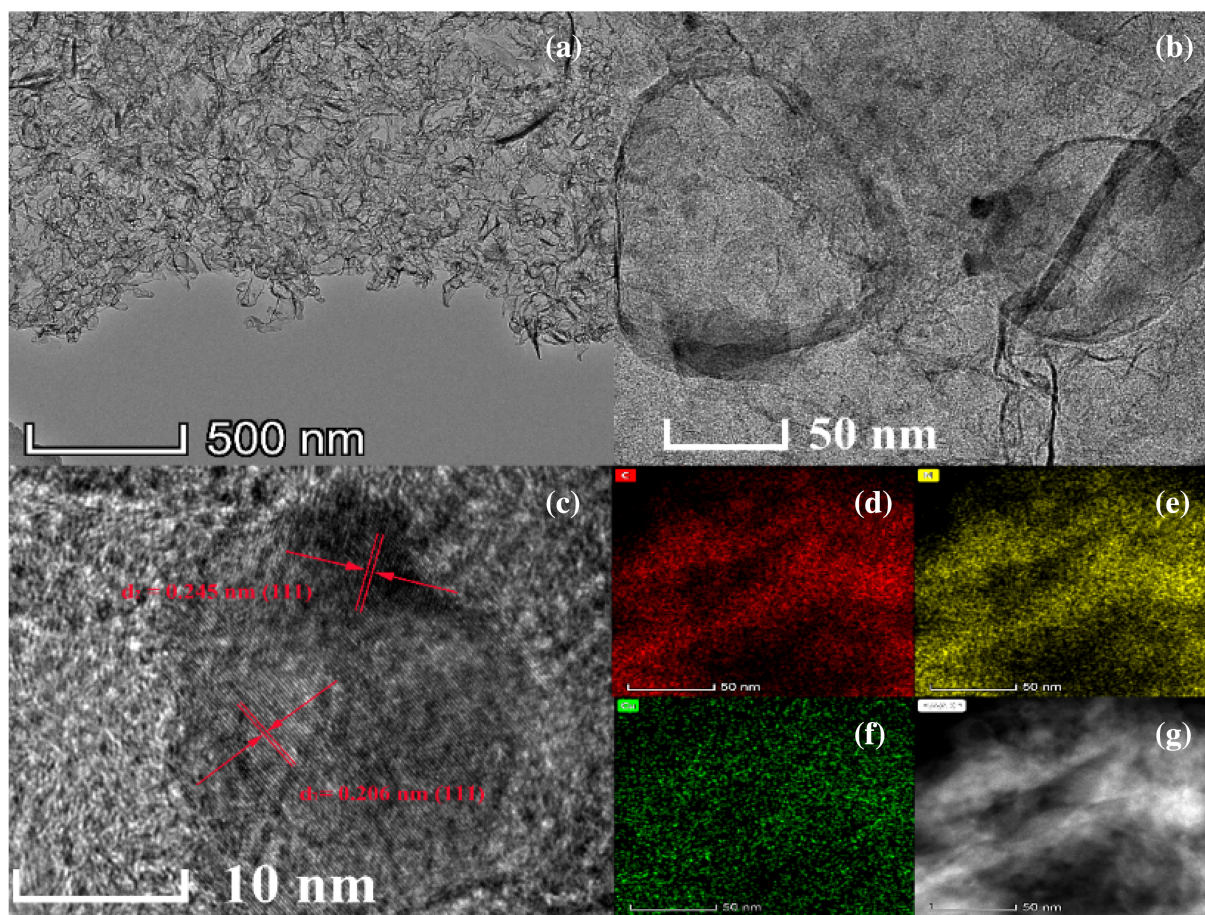


FIGURE 3 Effect of posttreatment on surface morphology, pore size, Cu loading, and distribution of catalyst. (a–c) Morphological characteristics of transmission electron microscopy (TEM) images at different magnifications. (d–f) The mapping of C, N and Cu. (g) A high-angle annular dark-field scanning transmission electron microscopy (HAADF-STEM) image of the Cu/CuO@CN(8)

particles are evenly dispersed on the carrier. Figure S5c is the measurement of the lattice after the cycle, which is consistent with the result of Figure 3c. The result of line scanning in Figure S5d reflects the proportion of catalyst Cu, C, and N content, which indirectly indicates that the content of Cu in the catalyst is less. In Figure S5e–S5h are images of C, N, Cu, and HAADF, respectively.

Additionally, owing to the surface area and pore size of the catalyst was closely related to the activity of the catalyst. Therefore, the characteristics of these corresponding aspects of the catalyst are investigated by BET. According to Figure 4, the micropore characteristics are investigated by nitrogen adsorption–desorption, and the particle size distribution of the catalyst and precursor is also illustrated. It can be found that the catalyst and the carrier have obvious hysteresis loops. In detail, the significant mesoporous properties are confirmed to have existed in CN and Cu/CuO@CN(8), and Figure 4a and Table 1 show that the pore width has fluctuated between 3 and 6 nm. In addition, Figure 4b reveals that the initial

amount at the beginning of adsorption is not 0, which is due to the microporous nature of the carbon material and catalyst. Besides, compared with Cu/CuO@CN(8), the initial amount of CN adsorption is larger, indicating that the CN material has a large pore volume, and the incorporation of Cu reduces the pore volume. The average values of pore width, surface area, and pore volume are also shown in Table 1, and the surface area of Cu/CuO@CN(8) is reduced by $34 \text{ m}^2 \text{ g}^{-1}$ compared to CN, indicating that the doped of Cu decreases the surface area. Both Cu/CuO@CN(8) and CN have considerable specific surface area values, but the difference is small because of the low copper loading. It can also be seen from Table 1 that the volume of CN is $0.75 \text{ cm}^3 \text{ g}^{-1}$, whereas the Cu/CuO@CN(8) is $0.60 \text{ cm}^3 \text{ g}^{-1}$, which indicates that the Cu nanoparticles are dispersed inside the pores of the carrier. Furthermore, the result of pore size analysis shows that a small amount of doped Cu has a slight effect on the pore size. Generally, the precursor and catalyst with large surface area, pore volume, and

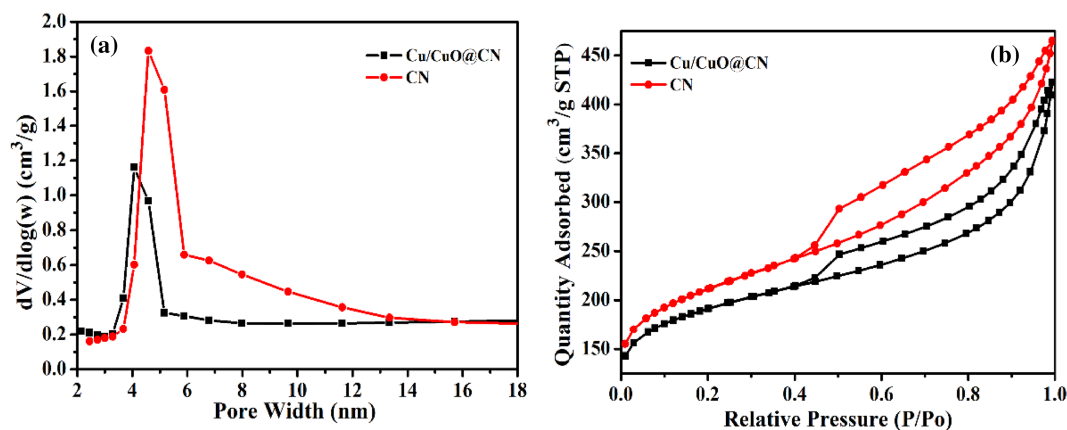


FIGURE 4 (a) Pore size distribution image of precursor and catalyst. (b) Nitrogen adsorption–desorption isotherms of CN and Cu/CuO@CN(8)

small pore width are synthesized. Indeed, the introduction of the Cu element mainly increases the active sites on the catalyst, thereby significantly improving the catalytic activity of the composite catalyst.

XPS is employed to determine the elemental composition and electronic state on the surface of the catalyst. The XPS full spectrum analysis of the Cu/CuO@CN (8) is shown in Figure 5a. It can be clearly verified that four elements of C, N, O, and Cu have existed in the catalyst. Distinctly, it is found that C, N, and O have strong peak intensities, and the binding energies of the corresponding peaks are close to 284.2, 394.7, and 528.55 eV, respectively.^[2a,11] Nevertheless, the peak intensity of Cu is weak and only 1.04% of Cu can be detected according to Table 2, which is mainly due to the fact that Cu particles are partially wrapped by the precursor. In detail, C mainly exists in the form of sp²-hybridized graphite C and CN bonds after high-temperature calcination, the high-resolution spectrum of C1s is shown in Figure 5b, which is split into three peaks of C–C (284.3 ± 0.2 eV), C=N (285.8 ± 0.2 eV), and C–N (287.6 ± 0.2 eV).^[10b,17] Because of the presence of the C–N bond, it is again demonstrated that the doped N atom has existed in the carbon matrix of the catalyst. Because the N atoms have a lone pair of electrons, it is theoretically possible to adjust the electron cloud density on the surface of the carbon material and increase the degree of disorder, which makes the CN bonds (C=N and C–N) shift to a higher energy level.^[10b,17,18] The fine

spectrum of N1s is illustrated in Figure 5c. It can be confirmed from the figure that there are three states of N in the catalyst, and the corresponding binding energy positions are 398.2, 399.8, and 401.3 eV, respectively.^[18a] The characteristic peaks of the low binding energy are assigned to pyridinic-N and pyrrolic-N, respectively. The peak at the higher binding energy (401.3 eV) is attributed to graphite-N, which existed in the π -conjugated system of lone pair electrons in carbon materials.^[2a,10b,18a] Indeed, it has been confirmed that N atoms can enhance electron transfer, thereby increasing the activity and stability of the catalyst. Therefore, it can be concluded that N atoms have been successfully doped into the carbon material and formed a CN bond.^[17,18] In addition, Figure 5d shows the high-resolution spectra of Cu. Although the peak intensity of Cu is relatively weak in full spectrum, a fine spectrum of Cu can still be obtained by analyzing. The characteristic peaks at the binding energy of 953.4 and 933.0 eV correspond to the 2p_{1/2} and 2p_{3/2} energy levels of zero-valent copper, respectively. Simultaneously, there is a satellite peak corresponding to each, and the characteristic peaks at 954.8 and 935.2 eV are attributed to 2p_{1/2} and 2p_{3/2} of the oxidized Cu²⁺, respectively.^[1f,2a,6] This is the result of oxygen in the air reacting with metal Cu in the catalyst after the catalyst is prepared, resulting in a small amount of elemental Cu being oxidized to CuO. Furthermore, this phenomenon is consistent with the XRD pattern results of Figure 1a.

TABLE 1 Nitrogen adsorption-desorption isotherms of CN and Cu/CuO@CN(8)

Sample	Average pore width (nm)	Surface area (m ² g ⁻¹)	Pore volume (cm ³ g ⁻¹)
CN	4.26	660.94	0.75
Cu/CuO@CN (8)	3.82	626.07	0.60

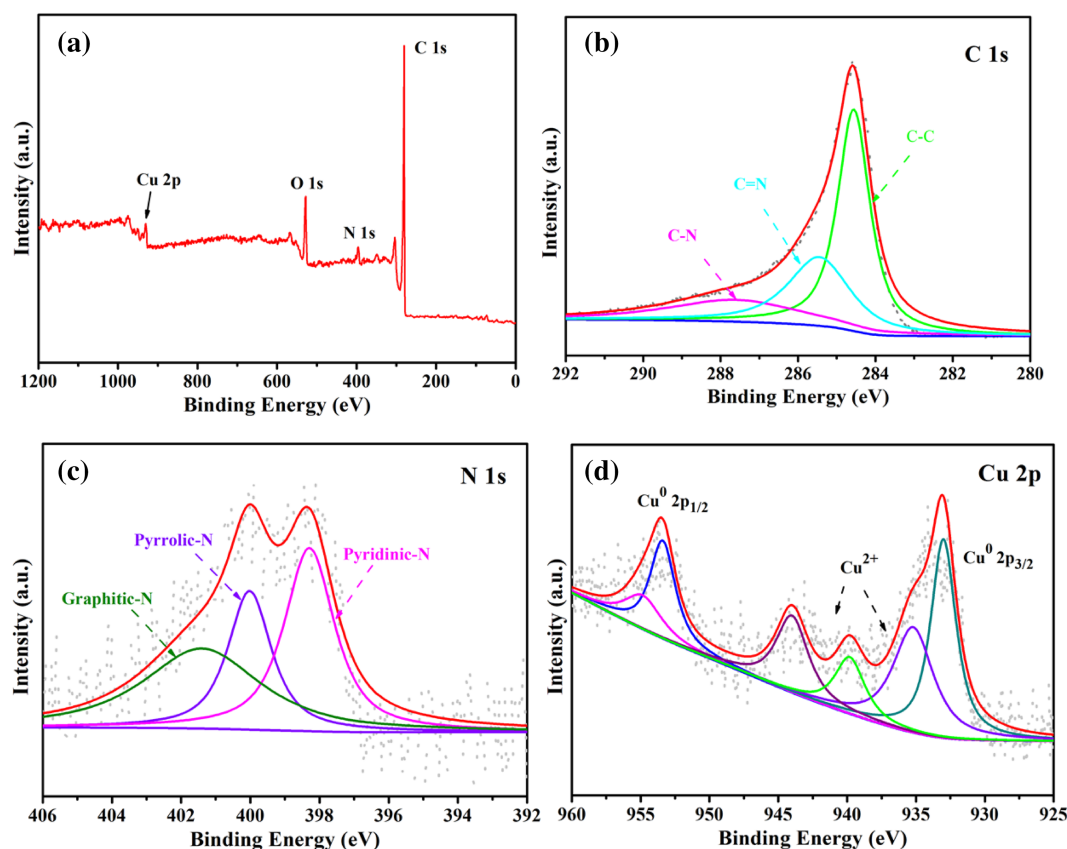


FIGURE 5 (a) Full spectrum analysis of X-ray photoelectron spectroscopy (XPS) data for the catalyst. (b-d) The high resolution XPS spectra corresponding to C 1s, N 1s, and Cu 2p in the catalyst, respectively

Sample	Carbon (%)	Nitrogen (%)	Oxygen (%)	Copper (%)
Cu/CuO@CN (8)	89.22	4.85	5.52	0.42
Cu/CuO(12%)@CN (8)	71.82	7.62	14.23	6.33

TABLE 2 The XPS analysis of the element content in Cu/CuO@CN (8) and Cu/CuO(12%)@CN (8)

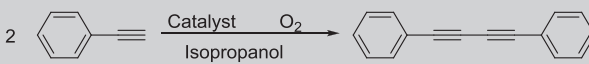
Abbreviation: XPS = X-ray photoelectron spectroscopy.

3.2 | Performance of catalysts

This study evaluates the catalytic performance of different catalysts for phenylacetylene coupling; a significant reaction is applied to the synthesis of organic monomers and fine chemicals. As illustrated in Table 3, Entries 1–4 demonstrate that the catalytic activity of the coupling reaction to phenylacetylene remains unchanged as the Cu content reduces. In detail, the 1,4-diphenylbutadiyne is obtained with a higher conversion of 99.9% and the turnover frequency (TOF) value of Cu/CuO@CN(8) catalyst is 96.8 h^{-1} . Entry 4 further indicates that low loadings (3.3%) can also satisfy catalytic activity of the reaction as measured by ICP-OES. Entries 4–7 show the comparison of the catalysts at different temperatures, demonstrating that Cu/CuO@CN (8) has a remarkable catalytic activity. In addition, copper salt catalysts of

different anions are contrasted as shown in Entries 9–12, from which it is known that the introduction of NO_3^- contributes to the catalytic reaction. In contrast, the influence of the catalyst activity with the N-based doped on the reaction is not negligible, as shown in Entries 4 and 8. According to the literature report and the experimental demonstration of the Entries 13 and 14, it is illustrated that Cu and CuO are also responsible for the coupling activity of phenylacetylene. Also, as shown in Entry 15, the blank experiment without adding catalyst was implemented once again to demonstrate the fact that Cu is the active center of the reaction.

At the same time, the bases are also one of the influencing factors of the coupling reaction. Therefore, different bases were compared to further explore the catalytic activity of the catalyst in this reaction, as shown in Table S2 in the supporting information. The presence of

TABLE 3 Catalytic activities of different catalysts


Entry	Catalyst	Time (h)	Temperature (°C)	Conversion ^a (%)	TOF (h ⁻¹)
1	Cu/CuO@CN(20%)	1	60	99.9	16
2	Cu/CuO@CN(12%)	1	60	99.9	26.7
3	Cu/CuO@CN(6.5%)	1	60	99.9	49.3
4 ^b	Cu/CuO@CN(8)	1	60	99.9	96.8
5 ^c	Cu/CuO@CN(9)	1	60	96	92.8
6 ^c	Cu/CuO@CN(7)	1	60	97.4	94.28
7 ^c	Cu/CuO@CN(6)	1	60	96.5	93.42
8 ^d	Cu/CuO@C(8)	1	60	98	94.84
9 ^e	Cu/CuO@CN(S)	10	25	96	9.29
10 ^e	Cu/CuO@CN(C)	10	25	95.2	9.21
11 ^e	Cu/CuO@CN (Cl)	10	25	96.3	9.32
12	Cu/CuO@CN(8)	10	25	98	9.48
13	Cu	6	25	87	16.3
14	CuO	10	25	70	9.68
15	—	10	60	trace	0

Note: Reaction condition: phenylacetylene (1 mmol), NaOH (2 eq.), catalyst (20 mg) solvent (2 ml), and O₂ balloon (1 atm).

Abbreviations: GC-MS = gas chromatography-mass spectrometry, ICP-OES = inductively coupled plasma optical emission spectrometer, TOF = turnover frequency.

^aDetermined by GC-MS.

^bThe mass fraction of Cu was 3.3 wt% as measured by ICP-OES.

^cThe different temperatures of calcination.

^dNo nitrogen source added.

^eThe different types of copper salts.

base is contributed to the detachment of the H protons in the terminal alkyne, thereby facilitating the rapid progress of the reaction system. Moreover, the inorganic base plays a major role in the experimental system under the conditions of isopropanol (IPA) as a solvent. In detail, it can be observed that the conversion rate increases with increasing alkalinity, and this is mainly due to the enhanced ability of the base to remove H protons. Then it is found that the effect of KOH and NaOH on the conversion of the reaction is not significant by comparing Entries 3 and 4. Therefore, NaOH was used as a base in this study. At the same time, we also did a blank comparison experiment, and it can be seen in Entry 11 of Table S2 that no base addition is inactive for the conversion of phenylacetylene. Similarly, we found that it is difficult to induce reactions when molecular oxygen is not introduced into the reaction system rather than relying on oxygen in the air (Entry 12, Table S2). The results show that the nitrogen heteroatom incorporated into carbon material facilitates the activation of O₂ to trigger the

occurrence of this reaction. So molecular oxygen is also one of the indispensable factors that affect the progress of the reaction.

To investigate the effect of the solvent on the catalyst, a large amount of polar or nonpolar organic liquid is used as a solvent to conduct catalytic experiments (Table 4). Importantly, the temperature is also selected as one of the critical conditions to the reaction process. As detailed in Entries 1–18 of Table 4, and the screening conditions for the solvent are carried out under conditions of a small amount of substrate (0.2 mmol), 10 h and 25°C. As well know that polar solvents have a great influence on this reaction, especially when alcohols are used as a solvent. Especially, it can be observed that tert-butanol (Entry 15) is considered as the most suitable solvent for the reaction comparison with glycol, methanol, acetone, DMF, CH₂Cl₂ and the like. At the same time, tert-butanol not only has distinguished sustainability but also has excellent solvent action. It is further worth mentioning that the conversion of tert-butanol and isopropanol to the

TABLE 4 Catalytic activities of Cu/CuO(3.3%)@CN(8) in different solvents^a and temperatures^b

Reaction scheme: 2 Phenylacetylene $\xrightarrow[\text{Solvent, O}_2]{\text{Catalyst, NaOH}}$ Diphenylacetylene

Entry	Solvent	Time (h)	Temperature (°C)	Conversion ^c (%)	TOF (h ⁻¹)
1	Isopropanol	10	25	95	2.03
2	Glycol	10	25	60	1.28
3	Methanol	10	25	92.4	1.97
4	Acetone	10	25	82.6	1.76
5	Ethanol	10	25	93	1.984
6	DMF	10	25	85.3	1.82
7	n-propanol	10	25	97	2.07
8	DMSO	10	25	29	0.618
9	THF	10	25	73	1.58
10	CH ₂ Cl ₂	10	25	79	1.685
11	CHCl ₃	10	25	87	1.856
12	1,4-dioxane	10	25	80	1.706
13	Toluene	10	25	63	1.344
14	Ethyl acetate	10	25	67	1.43
15	tert-Butanol	10	25	98	2.09
16	Hydrazine hydrate	10	25	80	1.71
17	H ₂ O	10	25	trace	0
18	—	10	25	trace	0
19 ^b	tert-Butanol	4	70	99.9	24.218
20 ^b	tert-Butanol	4	60	99.9	24.218
21 ^b	tert-Butanol	2	60	99.9	48.43
22 ^b	tert-Butanol	1.5	60	99.9	64.58
23 ^b	tert-Butanol	1	60	99.9	96.87
24 ^b	tert-Butanol	4	50	99.9	24.218
25 ^b	tert-Butanol	2	50	99.9	48.43
26 ^b	tert-Butanol	1	50	98.2	95.22
27 ^d	tert-Butanol	1	60	trace	0
28 ^e	tert-Butanol	1	60	trace	0

Abbreviations: GC-MS = gas chromatography-mass spectrometry, TOF = turnover frequency.

^aReaction condition: phenylacetylene (0.2 mmol), catalyst (20 mg), NaOH (20 mg), solvent (1 ml), and O₂ balloon (1 atm).

^bReaction condition: phenylacetylene (1 mmol), NaOH (2 eq.), catalyst (20 mg), tert-Butanol (2 ml), and O₂ balloon (1 atm).

^cDetermined by GC-MS.

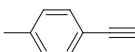
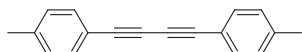
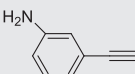
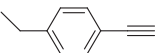
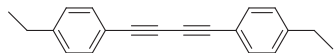
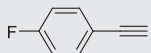
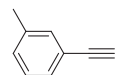
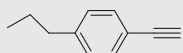
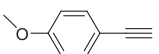
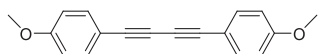
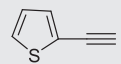
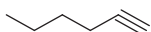
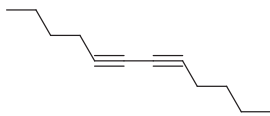
^dNo base.

^eNo O₂.

reaction is 98% (Entry 15) and 95% (Entry 1) under the same reaction conditions, which proves that tert-butanol is superior to isopropanol. In addition, TOF is also calculated accordingly. It can be concluded that when tert-butanol is used as a solvent, its TOF value is 2.07 (Entry 7) under the condition that phenylacetylene is 0.2 mmol.

Hence, we can draw a general conclusion that the electron-donating ability of tert-butyl is weaker than that of isopropyl, but from the point of view of acidity and alkalinity, the stronger the electron-donating ability of the electron-donating group, the weaker the acidity. In addition, considering that the experiment is implemented

TABLE 5 Coupling of different alkynes

Entry	Substrate	Product	Conversion ^a (%)
$2 \text{ R}-\text{C}\equiv\text{C} \xrightarrow[\text{tert-Butanol, O}_2]{\text{Catalyst, 60 }^\circ\text{C, 1 h}} \text{R}-\text{C}\equiv\text{C}-\text{C}\equiv\text{C}-\text{R}$			
1			97
2			96
3			99
4			96
5 ^b			99
6			98
7			99
8			99
9			72

Note: Reaction condition: phenylacetylene (0.2 mmol), catalyst (20 mg), NaOH (20 mg), solvent (1 ml), and O₂ balloon (1 atm) at 60°C for 2 h.

Abbreviation: GC-MS = gas chromatography-mass spectrometry.

^aDetermined by GC-MS.

^bReaction time: 1 h.

in an alkaline environment, so we make the final decision that uses tert-butanol as the best solvent and apply it to the reaction.

A suitable temperature is essential in terms of reducing reaction time and speeding up the reaction rate. In this way, the effect of temperatures on the coupling of phenylacetylene is also illustrated in Table 4 (Entries 19–28). Comparing the experimental results, 99.9% conversion can be achieved after 4 h at the initial set temperature of 70°C. However, with the continuous shortening of the reaction time and the lowering of the reaction temperature, we can find that the same conversion rate (99.9%) can be achieved after 1 h at 60°C and its TOF value is 96.87 (Entry 23). The conversion rate will be greatly reduced when the reaction temperature is further reduced. Therefore, the appropriate temperature for this experiment is 60°C.

By screening the above experimental conditions, the optimal reaction conditions for the coupling of phenylacetylene to 1,4-diphenylbutadiyne are Cu/CuO (3.3%)/CN(8) (20 mg), NaOH (2 eq.), tert-Butanol (2 ml), and O₂ balloon (1 atm) at 60°C for 1 h. In order to verify the general applicability of this experiment, some similar acetylenes are investigated as substrates under optimal experimental conditions and the results are shown in Table 5. The significant conversion (>95%) of most of the corresponding alkynes are achieved on the catalyst. Further, a platform substance (3-alkynyltoluene, 4-propylbenyne, 4-alkynylanisole, etc.) derived from a coupling substance (phenylacetylene) is carried out. As shown in Entries 5–7 in Table 5, the corresponding conversion rates are 99%, 98%, and 99%, respectively. Hence, it can be seen that the catalyst has a prominent catalytic effect on alkyne compounds with benzene ring. Carefully, it can be found that the catalytic coupling effect of the substrate with electron-pushing group on the benzene ring is more significant than that of the substrate with electron-withdrawing group on the benzene ring, by comparing Entries 3 and 4 and Entries 2 and 5. In addition, 2-ethynylthiophene also gave a good coupling yield of 99% (Entry 8). However, the conversion of n-hexyne is not satisfactory compared to the above substrates (only 72%). This may be attributed to the fact that the catalyst tends to form a π bond with benzene ring-containing substance, which facilitates electron transport and thereby enhances the reaction rate. Generally, the prepared catalyst of Cu/CuO@CN(8) has distinguished properties for coupling other acetylene compounds.

3.3 | Cycles of catalyst

In addition to excellent catalytic activity, a good heterogeneous catalyst should also have good recyclability and

reusability. The circulation capability of the catalyst is one of the necessary factors for its industrial production. Therefore, Cu/CuO@CN(8) was investigated in this experiment for the recyclability of phenylacetylene coupled to 1,4-diphenylbutadiyne, as shown in Figure 6. For the cycle results, it is clear that the conversion of the reaction exceeds 90% after five cycles of testing. In detail, the catalyst and the reaction system were separated by filtration after one reaction, and then the recovered catalyst was washed several times with ethanol and deionized water. Finally, the washed catalyst was thoroughly dried in a vacuum oven at 60°C for the subsequent cycle.

Furthermore, the filtered catalyst is collected after the cycle, and its metal content is slightly reduced by the ICP-OES, indicating that only a small amount of copper is separated from the catalyst. In addition, The FT-IR is implemented to structural analysis and identification of the catalyst. Figure 7 shows the infrared adsorption spectrum of the precursor and Cu/CuO@CN(8) on phenylacetylene. Clearly, it can be found that there are two new peaks at 748.2 and 686.4 cm⁻¹, indicating that the phenylacetylene was well adsorbed on the catalyst. Further, it is observed that the adsorption peak is slightly shifted after five cycles, and its corresponding positions are 756.0 and 693.1 cm⁻¹, respectively. This indicates that there is no significant change in the catalyst active after the catalyst is recycled, which reflects the excellent recyclability of the prepared catalyst.

3.4 | Kinetic study

To further understand the reaction mechanism, kinetic experiments are performed to study the phenylacetylene coupling reaction. In this experiment, the reaction kinetics of the coupling of phenylacetylene to 1,4-diphenylbutadiyne is studied by the speed-limiting step method. The specific conditions of the reaction are as follows: phenylacetylene (3 mmol), NaOH (200 mg), tert-butanol (6 ml), O₂ (1 atm), catalyst (10 mg), and reaction time (40 min). This experiment is studied by using models and basic assumptions of kinetic theory in heterogeneous catalysis. The details are as follows: The total reaction formula is defined as Equation (1), by which the total reaction rate Equation (2) can be derived. The residual substrate concentration and oxygen pressure in Equation (2) are represented by C_A and P , respectively, and the corresponding reaction order is represented by b and a . Because the pressure of O₂ is always maintained at 1 atm and its content is far excessive as the reaction proceeds, so $P_{(O_2)}$ is regarded as a constant. Hence, the total reaction rate equation can be approximated as

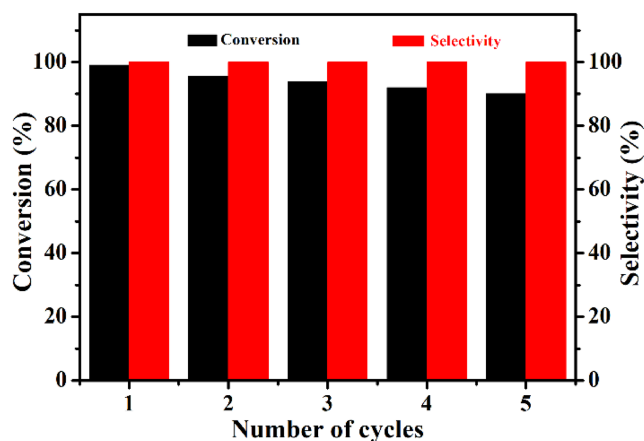


FIGURE 6 The recyclability and reusability of Cu/CuO@CN(8). Reaction condition: phenylacetylene (1 mmol), NaOH (2 eq.), catalyst (20 mg), tert-Butanol (2 ml) and O₂ balloon (1 atm) at 60°C for 1 h. The conversion is determined by gas chromatography–mass spectrometry (GC–MS)

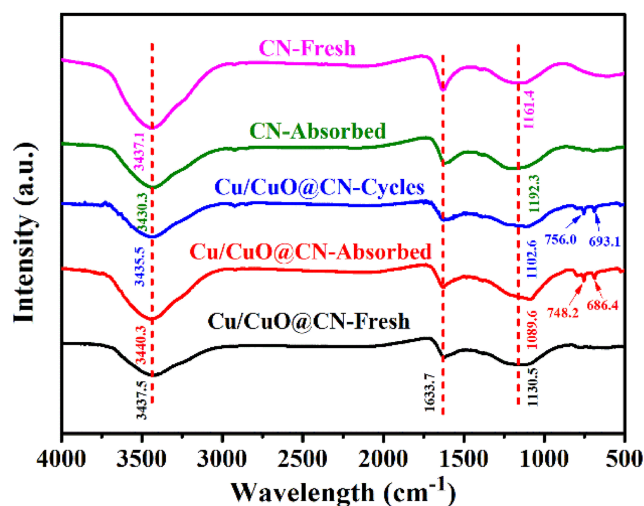
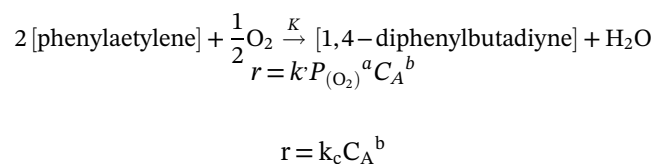


FIGURE 7 The Fourier-transform infrared spectroscopy (FT-IR) of catalyst and precursor

Equation (3). And the total reaction rate constant is expressed by k_c .



Next, the relationship between the reaction time and the conversion rate is shown in Figure 8a, and the value of b is 1.02 by linearly fitting of the remaining substrate concentration and reaction time in different time periods

(Figure 8b). Therefore, it can be concluded that the reaction conforms to the quasi-first-order kinetic equation. On the basis of the consistency of other conditions, the corresponding reaction rate constant k can be obtained only by changing the reaction temperature. Finally, the Arrhenius equation (Equations 4 and 5) can be used to determine the apparent activation energy E_a required for the reaction.

$$k_c = A e^{-E_a/RT}$$

$$\ln k_c = -\frac{E_a}{RT} + \ln A.$$

A , R , and T in the above equations are expressed as apparent frequency factors, molar gas constants, and thermodynamic temperatures, respectively. As shown in Figure 8c, a straight line with good fitting degree can be obtained by plotting a series of $(1/T, \ln k)$ experimental data, and the value of E_a can be deduced as 22.74 kJ mol⁻¹ according to the slope and intercept of the line. It is further proved that the conclusions of the kinetic study are in good agreement with the results of the reaction conversion rate. The above consequences fully demonstrate that the best catalyst has the lowest reaction activation energy, which again indicates that Cu/CuO@CN(8) is the best catalyst for the realization of phenylacetylene coupling.

3.5 | Mechanism research

Samples are characterized by the FT-IR and explained in combination with the mechanism schematic diagram to investigate the reaction mechanism of this experiment. Generally, Figure 7 shows that the characteristic absorption peaks of different types of catalysts are between 500 and 3500 cm⁻¹.^[10b] In detail, the catalyst (Cu/CuO@CN-Fresh) and the carrier (CN-Fresh) that are not in contact with the reaction substrate have similar characteristic absorption peaks, which indicates that the doping of metals does not cause changes in functional groups. In addition, this experiment further explored the infrared spectra of the catalyst (Cu/CuO@CN-Absorbed), the carrier (CN-Absorbed), and the catalyst after the cycle (Cu/CuO@CN-Cycles) in contact with the substrate. By comparison, it can be found that there are two new weak peaks in the range of 650–800 cm⁻¹, which may be due to the introduction of Cu improves the adsorption capacity of the catalyst to the substrate molecule (phenylacetylene). Therefore, it can be attributed to the out-of-plane bending vibration peak of the aromatic ring.

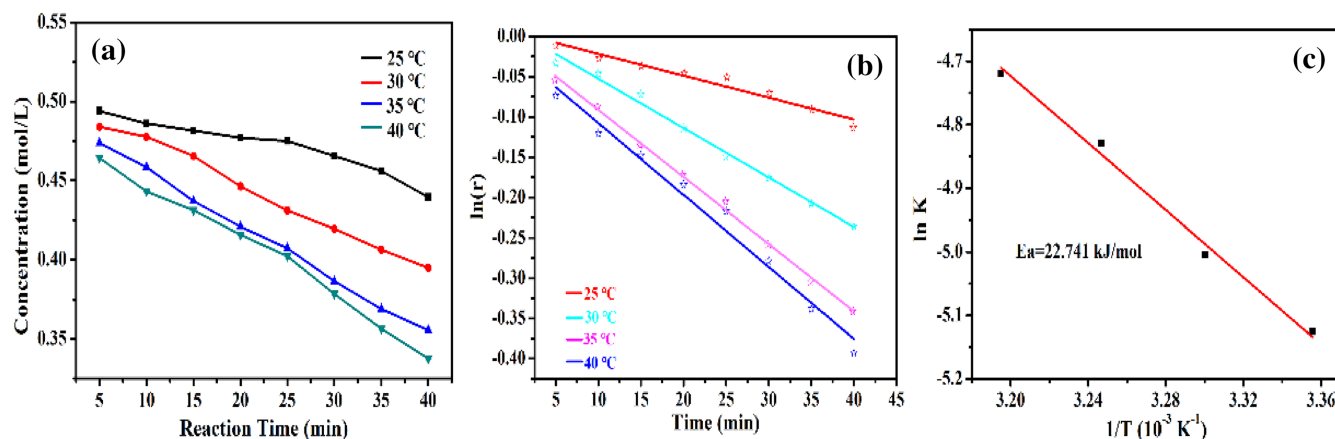
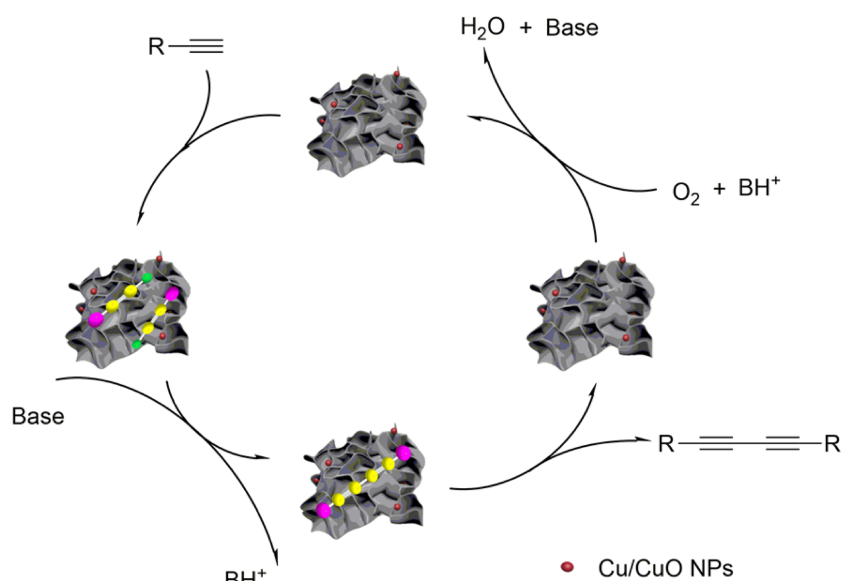


FIGURE 8 Kinetic study on the coupling of phenylacetylene

Furthermore, all catalysts and precursors have three strong absorption peaks. In detail, peaks with wave numbers in the range of 500–1200 cm^{-1} are assigned to C–C and C–N.^[10b,19] In the region of 1500–1650 cm^{-1} , the peaks of stretching vibration are mainly attributed to the C=N.^[10b,19,20] And the stretching vibration peak that can be assigned to the N–H bond in the region of 3400–3500 cm^{-1} .^[10b,19a,20]

In addition, the degree of graphitization is maximized ($I_D/I_G = 1.0243$) when the calcination temperature reaches 800 °C, which promotes the electron transfer between the catalyst and the substrate (Figure 1b). At the same time, a blank control experiment is conducted with nitrogen to study the role of oxygen as a metal oxide during the reaction (Entry 28, Table 4). The detailed mechanism inference is

shown in Scheme SCHEME 2. Initially, the H proton of the terminal alkyne is combined with the base and then detached, while Cu^0 is oxidized to Cu^+ by oxygen. Next, the oxidized Cu^+ is matched with the two substrates that have lost the H protons, then the reduction elimination is implemented with the production of products and the reduction of Cu^+ to Cu^0 .^[1a, e,10c] Ultimately, water is formed by the combination of H protons and oxygen, accompanied by the oxidation of Cu^0 to Cu^+ to promote the next cycle.^[3e,6,7e,10c] In the case of Cu^{2+} , it is reduced to Cu^+ after the reduction elimination process is implemented. Subsequently, the oxidation reaction is carried out as Cu^+ is oxidized to Cu^{2+} again. Moreover, the results of the cycle experiments demonstrate that the catalyst has a reliable ability to recycle.



SCHEME 2 Proposed reaction mechanism

4 | CONCLUSIONS

In summary, we demonstrate a mild and reliable metal precursor combination strategy for the synthesis of the flexible acetone carbon and full advantage of impregnation. The synthesis route in this experiment is a precursor formed by acetone and urea to immobilize the metal particles in space, which opens up a potential and advantageous way to realize the carrier of acetone. In addition, analysis of the experimental results and characterization indicates that the optimal catalyst Cu/CuO@CN(8) realized the coupling of phenylacetylene to 1,4-diphenylbutylene based on high conversion and excellent cycleability. Simultaneously, our model is also applicable to the coupling of acetylene groups in several alkynes, which have a remarkable catalytic effect on the tested metals (Pd and Cu) under the optimal reaction conditions. Nevertheless, the results exhibited Cu/CuO@CN(8) of low-load metal have certain advantages in this reaction, because it has the best affinity for such compounds. Specifically, the incorporation of nitrogen into the carbon material can significantly enhance the adsorption capacity of the catalyst. Besides, the outstanding catalytic performance of Cu/CuO@CN(8) with a low loading of Cu is also closely related to its large specific surface area, high porosity, exclusive porous structure, uniform distribution of Cu, CuO nanoparticles, and low thermodynamic energy. Ultimately, this work provides novel insights into the surface recombination of carbon-based acetone catalysts with high catalytic activity.

CONFLICT OF INTEREST

The authors declare no competing financial interest.

AUTHOR CONTRIBUTIONS

Lei Ma: Conceptualization; data curation; formal analysis; software; supervision; visualization. **Pengbo Jiang:** Software. **Kaizhi Wang:** Software. **Xiaokang Huang:** Software. **Ming Yang:** Software. **Li Gong:** Software. **Qi Jia:** Software. **Xiao Mu:** Software. **Yucong Xiong:** Software. **Rong Li:** Conceptualization; data curation; formal analysis; resources; visualization.

DATA AVAILABILITY STATEMENT

The data that support the findings of this study are available in the supporting information of this article.

ORCID

Lei Ma  <https://orcid.org/0000-0002-2778-0604>

Pengbo Jiang  <https://orcid.org/0000-0003-2745-7599>

Kaizhi Wang  <https://orcid.org/0000-0002-0277-8313>

Xiaokang Huang  <https://orcid.org/0000-0003-0339-1257>

Ming Yang  <https://orcid.org/0000-0002-3964-9830>

Li Gong  <https://orcid.org/0000-0001-7773-0958>

Rong Li  <https://orcid.org/0000-0003-1037-0841>

REFERENCES

- [1] a) S. T. Aziz, R. U. Islam, *Catal. Lett.* **2017**, *148*, 205; b) Z. Chen, R. Shen, C. Chen, J. Li, Y. Li, *Chem. Commun.* **2018**, *54*, 13155; c) T. P. Cheng, B. S. Liao, Y. H. Liu, S. M. Peng, S. T. Liu, *Dalton Trans.* **2012**, *41*, 3468; d) T. de Haro, C. Nevado, *Chem. Commun.* **2011**, *47*, 248; e) N. Devarajan, M. Karthik, P. Suresh, *Org. Biomol. Chem.* **2017**, *15*, 9191; f) F. Farzaneh, E. Rashtizadeh, *J. Iran. Chem. Soc.* **2016**, *13*, 1145.
- [2] a) W. Gao, S. Li, H. Huo, F. Li, Y. Yang, X. Li, X. Wang, Y. Tang, R. Li, *Mol. Catal.* **2017**, *439*, 108; b) W. Guo, S. Niu, W. Shi, B. Zhang, W. Yu, Y. Xie, X. Ji, Y. Wu, D. Su, L. Shao, *Cat. Sci. Technol.* **2018**, *8*, 2333; c) Z. Jia, K. Wang, T. Li, B. Tan, Y. Gu, *Cat. Sci. Technol.* **2016**, *6*, 4345.
- [3] a) B. Lai, Z. Huang, Z. Jia, R. Bai, Y. Gu, *Cat. Sci. Technol.* **2016**, *6*, 1810; b) A. S. Levashov, D. S. Buryi, O. V. Goncharova, V. V. Konshin, V. V. Dotsenko, A. A. Andreev, *New J. Chem.* **2017**, *41*, 2910; c) H. Li, M. Yang, Q. Pu, *Micropor. Mesopor. Mater.* **2012**, *148*, 166; d) S. Li, X. Chen, J. Chen, H. Gong, *B. Chem. Soc. Jpn.* **2016**, *89*, 794; e) X. Li, X. Liu, H. Chen, W. Wu, C. Qi, H. Jiang, *Angew. Chem. Int. Ed.* **2014**, *53*, 14485; f) G. Cahiez, A. Meyeux, J. Buendia, C. Duplais, *J. Am. Chem. Soc.* **2007**, *129*, 13788.
- [4] a) X. Li, D. Li, Y. Bai, C. Zhang, H. Chang, W. Gao, W. Wei, *Tetrahedron* **2016**, *72*, 6996; b) Q. Liu, L. Wu, R. Jackstell, M. Beller, *Nat. Commun.* **2015**, *6*, 5933.
- [5] a) B. D. C. Glaser, **1896**, *2*, 422; b) A. S. Hay, *J. Org. Chem.* **1962**, *27*, 3320.
- [6] W. Lu, W. Sun, X. Tan, L. Gao, G. Zheng, *Cat. Com.* **2019**, *125*, 98.
- [7] a) C. Meng, K. Yang, X. Fu, R. Yuan, *ACS Catal.* **2015**, *5*, 3760; b) S. B. Ötvös, Á. Georgiádes, R. Mészáros, K. Kis, I. Pálkó, F. Fülöp, *J. Catal.* **2017**, *348*, 90; c) A. Sagadevan, V. P. Charpe, K. C. Hwang, *Cat. Sci. Technol.* **2016**, *6*, 7688; d) X.-L. Shi, Q. Hu, F. Wang, W. Zhang, P. Duan, *J. Catal.* **2016**, *337*, 233; e) A. Toledo, I. Funes-Ardoiz, F. Maseras, A. C. Albéniz, *ACS Catal.* **2018**, *8*, 7495; f) S. Wang, D. Hu, W. Hua, J. Gu, Q. Zhang, X. Jia, K. Xi, *RSC Adv.* **2015**, *5*, 53935.
- [8] a) A. V. Zuraev, Y. V. Grigoriev, L. S. Ivashkevich, A. S. Lyakhov, O. A. Ivashkevich, *Z. Anorg. Allg. Chem.* **2017**, *643*, 1215; b) B. S. Chinta, B. Baire, *RSC Adv.* **2016**, *6*, 54449; c) X. Jia, K. Yin, C. Li, J. Li, H. Bian, *Green Chem.* **2011**, *13*, 2175.
- [9] a) S. Tang, L. Li, X. Ren, J. Li, G. Yang, H. Li, B. Yuan, *Green Chem.* **2019**, *21*, 2899; b) Y. Jian, M. Chen, B. Huang, W. Jia, C. Yang, W. Xia, *Org. Lett.* **2018**, *20*, 5370.
- [10] a) A. C. Uptmoor, J. Freudenberg, S. T. Schwabel, F. Paulus, F. Rominger, F. Hinkel, U. H. Bunz, *Angew. Chem. Int. Ed.* **2015**, *54*, 14673; b) K. Wang, P. Jiang, M. Yang, P. Ma, J. Qin, X. Huang, L. Ma, R. Li, *Green Chem.* **2019**, *21*, 2448; c) H. Xu, K. Wu, J. Tian, L. Zhu, X. Yao, *Green Chem.* **2018**, *20*, 793.

- [11] X. Huang, X. Wang, P. Jiang, K. Lan, J. Qin, L. Gong, K. Wang, M. Yang, L. Ma, R. Li, *Inorg. Chem. Front.* **2019**, *6*, 1482.
- [12] a) M. Fabre, J. Bonvoisin, *J. Am. Chem. Soc.* **2007**, *129*, 1434; b) X. Li, X. Xie, N. Sun, Y. Liu, *Angew. Chem. Int. Ed.* **2017**, *56*, 6994; c) Y. Liu, N. Gu, P. Liu, J. Xie, X. Ma, Y. Liu, B. Dai, *Appl. Organomet. Chem.* **2015**, *29*, 736.
- [13] L.-J. Zhang, Y.-H. Wang, J. Liu, M.-C. Xu, X.-M. Zhang, *RSC Adv.* **2016**, *6*, 28653.
- [14] X. Fan, N. Li, T. Shen, X.-M. Cui, H. Lv, H.-B. Zhu, Y.-H. Guan, *Tetrahedron* **2014**, *70*, 256.
- [15] a) M. Y. Kang, Y. Guo, H. Shi, M. S. Ye, B. Zhang, *ChemistrySelect* **2018**, *3*, 7054; b) N. Orozco, G. Kyriakou, S. K. Beaumont, J. Fernandez Sanz, J. P. Holgado, M. J. Taylor, J. P. Espinós, A. M. Márquez, D. J. Watson, A. R. Gonzalez-Eliphe, R. M. Lambert, *ACS Catal.* **2017**, *7*, 3113.
- [16] a) S. B. Patel, D. V. Vasava, *ChemistrySelect* **2018**, *3*, 471; b) Y. Shi, R. Yue, Y. Zhang, S. Lv, L. Bai, C. Zhang, X. Wen, *Cat. Com.* **2019**, *124*, 103.
- [17] H. K. Jeong, Y. P. Lee, R. J. Lahaye, M. H. Park, K. H. An, I. J. Kim, C. W. Yang, C. Y. Park, R. S. Ruoff, Y. H. Lee, *J. Am. Chem. Soc.* **2008**, *130*, 1362.
- [18] a) Z.-H. Sheng, L. Shao, J.-J. Chen, W.-J. Bao, F.-B. Wang, X.-H. Xia, *ACS Nano* **2011**, *5*, 4350; b) A. G. P. Ayala, T. Gemming, B. Büchner, M. H. Rummeli, D. Grimm, J. Schumann, R. Kaltofen, F. L. Freire Jr., H. D. Fonseca Filho, T. Pichler, *Chem. Mater.* **2007**, *19*, 6131.
- [19] a) H.-C. Ma, J.-L. Kan, G.-J. Chen, C.-X. Chen, Y.-B. Dong, *Chem. Mater.* **2017**, *29*, 6518; b) I. S. Pieta, A. Rathi, P. Pieta, R. Nowakowski, M. Hołdyski, M. Pisarek, A. Kaminska, M. B. Gawande, R. Zboril, *Appl. Catal. Environ.* **2019**, *244*, 272.
- [20] T. S. Miller, A. B. Jorge, T. M. Suter, A. Sella, F. Corà, P. F. McMillan, *Phys. Chem. Chem. Phys.* **2017**, *19*, 15613.

SUPPORTING INFORMATION

Additional supporting information may be found online in the Supporting Information section at the end of this article.

How to cite this article: Ma L, Jiang P, Wang K, et al. High-efficiency catalyst for copper nanoparticles attached to porous nitrogen-doped carbon materials: Applied to the coupling reaction of alkyne groups under mild conditions. *Appl Organomet Chem.* 2021;35:e6163. <https://doi.org/10.1002/aoc.6163>